Data Test of a Hydro-Kinematic State Graph for Landslide Forecasting

Mohit Sheode*

Department of Civil Engineering, Maulana Azad National Institute of Technology Bhopal, India

*Corresponding author: mhtsht@gmail.com

ORCID: https://orcid.org/0009-0009-5719-5084

Abstract

A graph model can make landslide-monitoring relationships explicit, but a graph is not automatically more informative than a well-regularized time-series model. This study tests that distinction on the publicly released Lamosano landslide record from northeastern Italy. The processed dataset contains 161 observations of 11-day horizontal InSAR differential displacement and rainfall from 10 April 2015 to 3 February 2020. Each graph node represents a causal hydro-kinematic state assembled from recent displacement, rainfall, trend, variability, and antecedent rainfall. Edges link a query state only to similar states in the preceding training record; the next displacement is estimated from their distance-weighted successors. Lookback and neighborhood size were selected by three blocked validation folds within the first 100 observations. The final 61 observations were held out chronologically. Climatology, persistence, and Ridge-ARX were tested under the same boundary. The selected graph produced a test RMSE of 2.451 mm and standard R^2 of −0.001, compared with 2.400 mm and 0.039 for Ridge-ARX. A 5,000-replicate moving-block bootstrap placed the graph-minus-ridge RMSE difference between −0.084 and 0.200 mm. Neither model recalled any of seven high-motion intervals. Thus, the graph exposed recurring monitoring states but did not supply dependable incremental forecast skill. The contribution is an auditable negative benchmark: with one monitoring point and a short record, state-graph complexity should not be interpreted as spatial knowledge or operational warning capability.

Keywords: causal state graph; InSAR; landslide displacement; open data; rainfall; time-series validation

1. Introduction

Graph learning is attractive in slope monitoring because the objects of interest are connected. Fractures intersect, instruments sample parts of the same moving mass, runoff follows terrain, and deformation propagates through material whose structure matters. A graph can encode these relations as nodes, edges, directions, and weights. It can also hide a weak assumption behind an impressive diagram. If edges are drawn from convenience rather

Journal-status statement: It is not under-review at any journal. Subsequent versions may contain substantial revisions arising from community feedback / submission to journal(s). Co-author(s) may be included in future versions. Feedback is welcome. Please feel free to contact the author (via email only). PRE-PRINT VERSION (I): 25.08.2026

THIS MANUSCRIPT IS A NON-PEER-REVIEWED PREPRINT SUBMITTED TO EARTHARXIV.

than geology, hydrology, measurement geometry, or strictly causal similarity, graph computation does not repair the representation.

Sheode [1] framed this issue for slope instability and landslide kinematics. That paper is the conceptual foundation for the present study: it separates physical, geomorphic, monitoring, and learning graphs and argues that their value depends on defensible nodes and edges, uncertainty-aware topology, temporal and spatial holdouts, and comparisons with non-graph baselines. The immediate empirical question is therefore narrower than "Can a graph neural network fit displacement?" *It is whether a stated graph representation adds information under a leakage-resistant test.*

Recent landslide-forecasting studies have used spatial graphs across GNSS stations. Jiang et al. [2] coupled graph convolution with a gated recurrent unit to learn spatial and temporal dependencies; Kuang et al. [3] used an attentive graph neural network; and Li et al. [4] introduced a dynamic graph optimized for multi-station GNSS monitoring. These studies illustrate the value of spatially distributed sensors. They also define a boundary: a record from one selected InSAR point cannot support claims about slope-wide spatial dependence. Treating lags or variables as if they were field-monitoring locations would create a graph, but not the graph implied by the site.

The open Lamosano dataset released by Nava et al. [5] provides a useful stress test. The site is a rotational, slow-moving landslide in Chies D'Alpago, northeastern Italy. Its reported volume is about 4.5×10^6 m^3, and its geological setting includes schistose clayey marls, greyish sandstone, and a sandy-gravel cover [5], [6], [7]. Nava et al. derived the horizontal displacement series from ascending and descending Sentinel-1 observations processed by the Small Baseline Subset approach [5], [8]. Their public processed file contains rainfall and differential displacement at an 11-day step. It is long enough for a chronological holdout, yet small enough that elaborate models can easily be tuned to idiosyncrasies.

Nava et al. [5] compared seven deep-learning architectures at four landslides and made the processed records public. At Lamosano, their reported test RMSE values ranged from

Journal-status statement: It is not under-review at any journal. Subsequent versions may contain substantial revisions arising from community feedback / submission to journal(s). Co-author(s) may be included in future versions. Feedback is welcome. Please feel free to contact the author (via email only). PRE-PRINT VERSION (I): 25.08.2026

2.070 to 2.424 mm. Those published scores are important context, but they are not treated here as rerun baselines: the training procedures differ, and their reported R^2 is the squared Pearson correlation, whereas this study uses the standard coefficient of determination, $1 - SSE/SST$. Mixing those quantities would make the ranking look more certain than it is.

This article extends the graph-representation framework through a deliberately small empirical test. Each node is a hydro-kinematic state of the monitored point, and each edge links that state to similar states observed earlier. The graph is causal, reproducible, and modest in scope. Three questions govern the analysis:

i. Does the state graph reduce unseen one-step forecast error relative to climatology, persistence, and a regularized autoregressive model with exogenous rainfall?
ii. Does any apparent graph advantage survive dependent-data resampling and reasonable changes in topology?
iii. Does average error conceal failure during the largest displacement intervals?

The central contribution is not a new deep architecture. It is a falsifiable open-data benchmark with a frozen test boundary, a claim-evidence map, and executable code. A null or negative comparison is informative here because it identifies the data conditions under which graph structure remains descriptive rather than predictive.

2. Research significance

Graph-based landslide models are often evaluated after numerous choices about windows, edges, thresholds, and network depth. With a short time series, those choices can consume the same evidence later used to claim success. This study fixes the evidentiary roles before model fitting: the first 100 observations support scaling, blocked validation, and final fitting; the remaining 61 support one final comparison. The training-state graph is frozen at the boundary. Earlier test observations may enter later test windows, as they would in rolling one-step monitoring, but test targets never select a model or become graph exemplars.

Journal-status statement: It is not under-review at any journal. Subsequent versions may contain substantial revisions arising from community feedback / submission to journal(s). Co-author(s) may be included in future versions. Feedback is welcome. Please feel free to contact the author (via email only). PRE-PRINT VERSION (I): 25.08.2026

THIS MANUSCRIPT IS A NON-PEER-REVIEWED PREPRINT SUBMITTED TO EARTHARXIV.

Table 1 states the resulting claim boundaries. The design permits a claim about one processed series, one forecast horizon, and one class of similarity graph. It does not permit inference about internal slip-surface connectivity, rainfall causation, transfer to another landslide, or operational early warning. This distinction is especially relevant for geotechnical practice, where a visually coherent network can be mistaken for physical validation.

Table 1. Evidence-to-claim map fixed before the final test

Question	Evidence used	Permitted claim	Deliberate non-claim
Dataset identity	Public CSV, source paper, checksum	Results refer to the released Lamosano point series	Raw Sentinel-1 processing was independently repeated
Graph validity	Causal state definition and training-only edges	Similar prior hydro-kinematic states are explicitly represented	Edges are physical cracks, flow paths, or slope-wide sensor links
Forecast comparison	Final 61 observations, common horizon and metrics	Relative one-step error on this chronological holdout	Universal superiority of graph or linear models
Uncertainty	Moving-block bootstrap of test residual pairs	Sampling range for RMSE and graph-minus-ridge difference	Formal proof of equivalence or stationarity
High-motion behavior	Training-defined 90th-percentile threshold	Ability to reproduce large intervals under a fixed rule	Calibrated alarm probability or safe warning threshold

3. Materials and methods

3.1 Public processed data and study boundary

The analysis uses `Data/df.csv` from the public repository accompanying Nava et al. [5]. The file was accessed on 21 August 2026. Its SHA-256 digest is `b16b0698201ca21409726645eb8963b950bd7371bfebb6fd2540226ccdaacb4e`, which fixes the exact input used here. The table has 161 complete rows and three columns: date, `p5`, and `rain`. In the released data, `p5` is processed horizontal differential InSAR displacement in millimetres per 11-day interval, and `rain` is accumulated rainfall in millimetres over the same interval. The dates span 10 April 2015 to 3 February 2020 (Fig. 1).

The source study reports that the displacement series was obtained from 229 ascending and 249 descending C-band Sentinel-1 images using SBAS processing in SARscape [5], [8]. The present work begins from the released processed CSV; it does not claim to reproduce that upstream interferometric processing. This matters for the meaning of “open”: the forecasting code and software stack are open source, and the processed table is publicly downloadable, but the source repository did not display a standalone data-licence file at the access date. The replication script therefore downloads and verifies the source file rather than republishing it.

Observations 0–99, ending on 3 April 2018, form the development period. Observations 100–160, beginning on 14 April 2018, form the untouched final test. The same 100/61 chronological boundary was retained from the source benchmark to preserve site-specific comparability [5]. The task is rolling one-step forecasting: at date t + 1, measurements available through date t may be used. Consequently, later test inputs can contain earlier observed test values. The forecast library, scalers, model settings, and event threshold remain fixed from training data.

Journal-status statement: It is not under-review at any journal. Subsequent versions may contain substantial revisions arising from community feedback / submission to journal(s). Co-author(s) may be included in future versions. Feedback is welcome. Please feel free to contact the author (via email only). PRE-PRINT VERSION (I): 25.08.2026

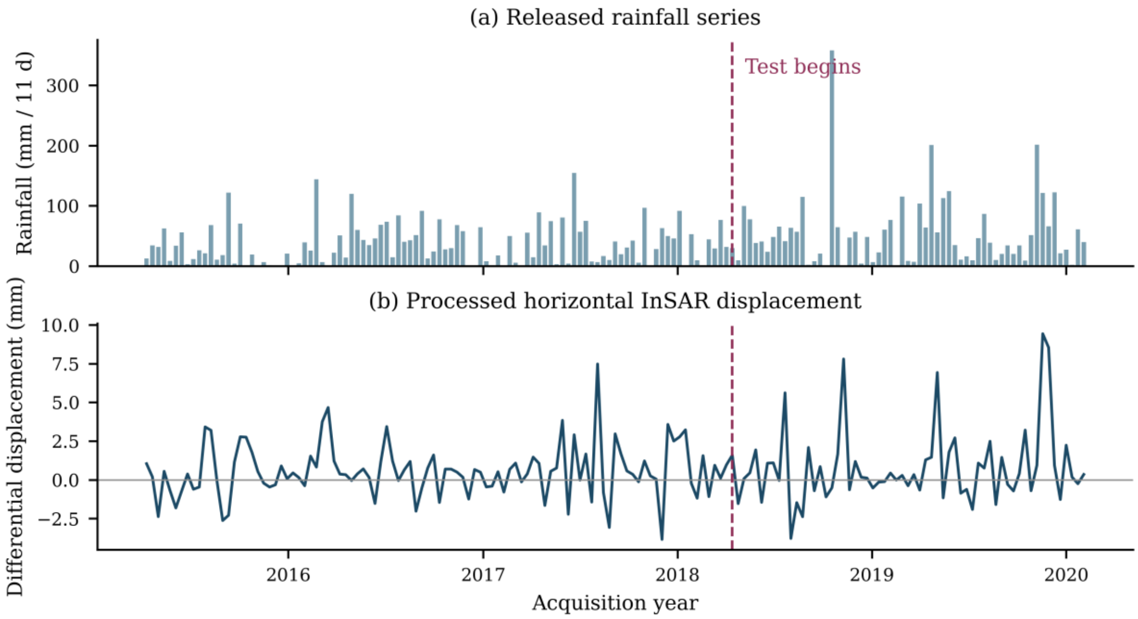

Fig. 1. Public Lamosano record and chronological development/test boundary. Rainfall and horizontal differential InSAR displacement are plotted at the released 11-day sampling interval.

3.2 Causal hydro-kinematic state graph

The single monitoring point rules out a spatial sensor graph. Instead, node i represents a state window ending at time t. For lookback w, the raw part of the state contains the previous w displacement values and w rainfall values. Six descriptors are appended: mean displacement, displacement standard deviation, least-squares displacement trend, rainfall sum, maximum rainfall, and an antecedent rainfall index. The latter is

$$\mathrm{ARI}(t) = \Sigma\ (l = 0 \text{ to } w - 1)\ 0.8^{l}\ r\ (t - l), \quad (1)$$

where r is 11-day rainfall. The decay was fixed before validation. These quantities create a hydro-kinematic state vector rather than a physical slope node. All features are transformed by a robust scaler fitted only to the applicable training fold, using its median and interquartile range.

For a query state q, Euclidean distance d (q, i) is calculated to eligible preceding states i. The k nearest states form directed query edges. Their weights are

$$a\,(q, i) = \exp\,[-\,\{d\,(q, i)/\mathrm{median}\,(d\,(q, Nq))\}^{\,2}],\ i \in Nq, \tag{2}$$

where Nq is the k-state neighborhood. The one-step prediction is the normalized weighted mean of the successors associated with those states:

$$\hat{y}(q) = \{\Sigma\,(i \in Nq)\ a\,(q, i)\ y(i{+}1)\}\,/\,\{\Sigma\,(i \in Nq)\ a\,(q, i)\}. \tag{3}$$

This construction is related to nearest-neighbor regression [9], but its graph form makes the representation auditable: nodes are states, edges are similarity relations, topology is controlled by k, and the label is the next observed displacement. No message-passing neural network is fitted because 97 eligible training states do not justify a parameter-heavy graph encoder.

Candidate lookbacks were $w \in \{3, 5, 7, 9, 12\}$; these correspond to 33–132 days. Candidate neighborhood sizes were $k \in \{3, 5, 7, 9, 12, 15, 20\}$. Settings were selected by mean RMSE across three forward blocked validation intervals with target indices 55–69, 70–84, and 85–99. Each fold was fitted only on observations preceding its validation block. Once selected, the graph was rebuilt from all development data and frozen. Figure 2a shows an undirected symmetrized view of the training topology in two principal-component dimensions for visualization only; principal components did not enter the forecast.

3.3 Baselines, diagnostics, and evaluation

Three baselines were chosen to test increasingly specific explanations. Climatology predicts the mean displacement in the first 100 observations. Persistence predicts the most recently observed displacement. Ridge-ARX uses the same state variables as the graph and fits ridge regression, thereby testing whether graph neighborhoods add value beyond regularized linear memory and rainfall covariates. Ridge lookback and penalty $\alpha \in \{0.01, 0.1, 1, 10, 100, 1000\}$ were chosen using the same blocked folds.

Performance is reported as mean absolute error (MAE), root-mean-square error (RMSE), and the standard coefficient of determination:

$$R^2 = 1 - \Sigma\,(y - \hat{y})^{\,2}\,/\,\Sigma\,(y - \bar{y})^{\,2}. \tag{4}$$

Journal-status statement: It is not under-review at any journal. Subsequent versions may contain substantial revisions arising from community feedback / submission to journal(s). Co-author(s) may be included in future versions. Feedback is welcome. Please feel free to contact the author (via email only). PRE-PRINT VERSION (I): 25.08.2026

THIS MANUSCRIPT IS A NON-PEER-REVIEWED PREPRINT SUBMITTED TO EARTHARXIV.

Because adjacent 11-day observations are dependent, independent-row bootstrap intervals would be too optimistic. A circular moving-block bootstrap [10] with block length five, 5,000 replicates, and random seed 84294 was applied to paired observations and predictions. It produced 95% percentile intervals for each RMSE and for the graph-minus-ridge RMSE difference. The interval is an uncertainty diagnostic, not a formal equivalence test.

High-motion intervals were defined before opening the test results as |p5| at or above the 90th percentile of absolute training displacement. The fixed threshold was 3.086 mm and identified seven test observations. Event RMSE, recall, precision, and maximum predicted displacement were recorded. This secondary analysis asks whether an acceptable average can coexist with missed movements.

Rainfall-displacement association was inspected only on the development period. Spearman correlation was calculated for rainfall leads of 0–66 days against signed displacement and displacement magnitude. The diagnostic does not establish causation; it checks whether a single monotonic lag dominates. After the primary model had been fixed, all 35 combinations of w and k were evaluated on the test period as a labeled post-hoc topology sensitivity analysis. Those values were not used to reselect the reported model.

The complete analysis was executed with Python 3 and open-source packages: NumPy 2.3.5 [11], pandas 2.2.3, SciPy 1.17.0 [12], scikit-learn 1.8.0 [13], and Matplotlib 3.10.8 [14]. The accompanying MIT-licensed script verifies the source hash, reconstructs every split and feature, reruns selection and testing, and writes the figures and machine-readable result tables.

4. Results

4.1 Development-period signal and selected topology

The released series is dominated by small 11-day changes interrupted by a few larger movements (Fig. 1). Rainfall also arrives in pulses, but the development-period lag diagnostic was weak and non-monotonic. For signed displacement, Spearman ρ ranged from −0.218 at a

Journal-status statement: It is not under-review at any journal. Subsequent versions may contain substantial revisions arising from community feedback / submission to journal(s). Co-author(s) may be included in future versions. Feedback is welcome. Please feel free to contact the author (via email only). PRE-PRINT VERSION (I): 25.08.2026

33-day lead to 0.270 at 22 days. For displacement magnitude, the largest value was 0.203 at 44 days (Fig. 2b). These correlations do not support a single rainfall lag as a stable control variable in this record.

Blocked validation selected w = 3 and k = 5 for the state graph, with a mean validation RMSE of 1.792 mm. Ridge-ARX selected w = 5 and α = 1000, with 1.813 mm. Thus, before the final test, the graph held a small 0.021-mm validation advantage.

The selected training graph contained 97 states and 349 undirected edges. It was one connected component, with density 0.075, mean degree 7.20 (range 5–12), and mean local clustering coefficient 0.395. The first two visualization components explained 28.4% and 24.0% of standardized feature variance. Figure 2a shows local grouping, but next-displacement colors overlap across much of the graph. Similar current states therefore did not map to sharply separated successors.

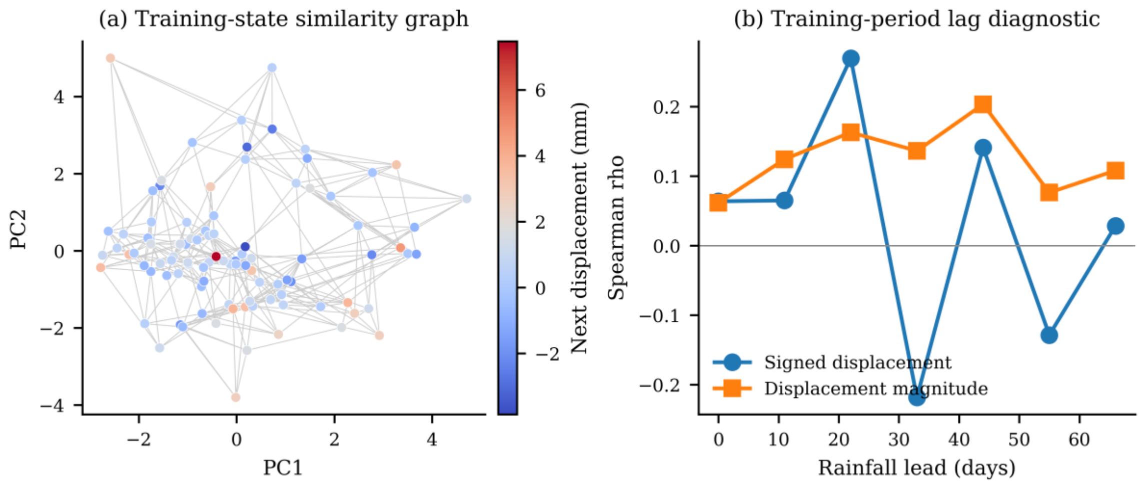

Fig. 2. Training-only diagnostics. (a) Symmetrized five-nearest-state graph projected into two principal components and colored by next displacement; projection is for display, not modeling. (b) Spearman association between training rainfall and later signed displacement or displacement magnitude.

4.2 Chronological test performance

The final 61-observation test reversed the small validation ordering (Table 2). Ridge-ARX had the lowest overall RMSE, 2.400 mm, followed by the state graph at 2.451 mm and climatology at 2.461 mm. Persistence was poorer at 3.290 mm because a large observed interval was often carried into the following, smaller interval. Standard R^2 was 0.039 for Ridge-ARX, −0.001 for the graph, −0.010 for climatology, and −0.806 for persistence. In practical terms, neither learned model explained much of the unseen variation.

The 95% moving-block RMSE intervals were broad and overlapped: 1.546–3.203 mm for Ridge-ARX and 1.589–3.230 mm for the graph. More directly, the bootstrap interval for graph RMSE minus ridge RMSE was −0.084 to 0.200 mm. The data are compatible with a small advantage for either model; they do not support a dependable graph improvement.

Table 2. One-step performance on the untouched 61-observation test

Model	MAE (mm)	RMSE (mm)	95% block-bootstrap RMSE (mm)	R^2	Event RMSE (mm)	Event recall
Climatology	1.609	2.461	1.574–3.299	−0.010	6.412	0.000
Persistence	2.338	3.290	2.397–4.057	−0.806	6.195	0.286
Ridge-ARX	1.580	2.400	1.546–3.203	0.039	6.201	0.000
State graph	1.664	2.451	1.589–3.230	−0.001	6.095	0.000

Figure 3 explains the weak scores. Ridge-ARX and the state graph tracked the low-amplitude center of the record, but both compressed the range. The observed test maximum was 9.428 mm. The graph's largest prediction was 2.676 mm and the ridge model's was 1.118 mm. Smooth central predictions lowered error on common intervals while erasing the movements most relevant to warning.

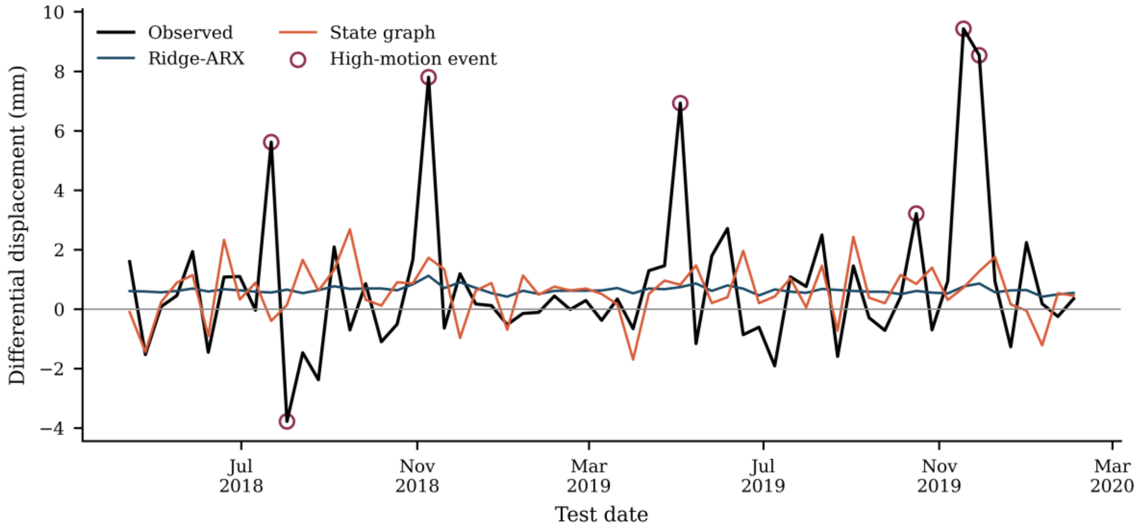

Fig. 3. Observed and predicted displacement in the chronological test. Open circles mark seven high-motion observations defined by the training-period 90th percentile of absolute displacement.

4.3 High-motion and topology checks

For the seven high-motion observations, event RMSE remained above 6.09 mm for every model (Table 2). The graph and Ridge-ARX recalled none because neither crossed the 3.086-mm event threshold. Persistence recalled two of seven events, but it also generated false positives and had the worst overall error. This is not evidence that persistence is a useful alarm; it shows that carrying a recent extreme value can cross a threshold even when timing is wrong.

Post-hoc topology sensitivity did not reveal a hidden robust neighborhood (Fig. 4b). Test RMSE changed with both lookback and k, and several unselected combinations happened to score better than the validation-selected topology. Choosing one of them after seeing the test would be leakage. The variation instead shows how easily a short record can reward a different graph definition depending on the inspected period.

Journal-status statement: It is not under-review at any journal. Subsequent versions may contain substantial revisions arising from community feedback / submission to journal(s). Co-author(s) may be included in future versions. Feedback is welcome. Please feel free to contact the author (via email only). PRE-PRINT VERSION (I): 25.08.2026

THIS MANUSCRIPT IS A NON-PEER-REVIEWED PREPRINT SUBMITTED TO EARTHARXIV.

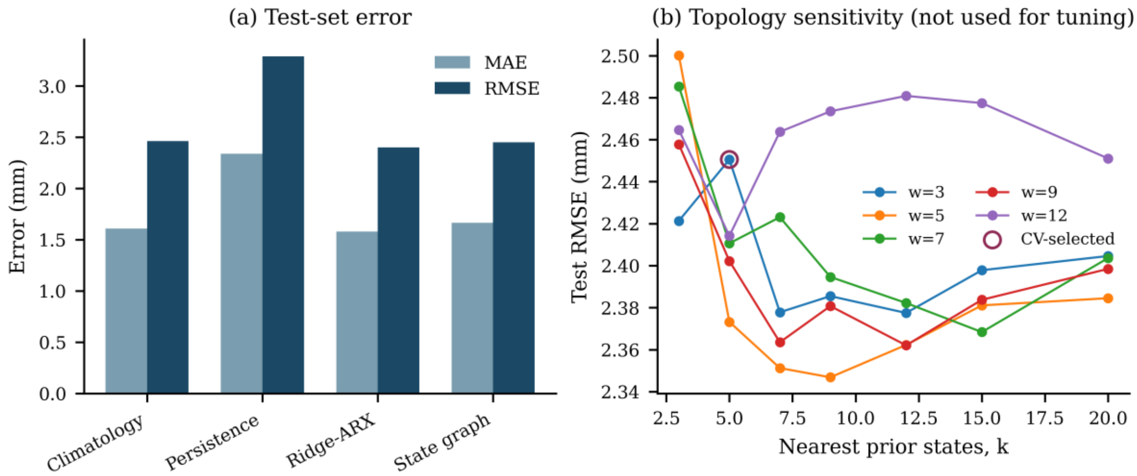

Fig. 4. Performance and sensitivity. (a) Test MAE and RMSE for all models. (b) Post-hoc state-graph test RMSE across lookback w and neighborhood k; the circled point is the setting selected without test access.

5. Discussion

5.1 What the graph added—and what it did not

The graph added an explicit representation of recurring hydro-kinematic states. Its connected, clustered topology showed that the development period contains local analogues rather than isolated observations. That is useful for inspection: an engineer can retrieve which prior states supported a forecast and examine their successor movements. The model is also parsimonious and deterministic.

What it did not add was reliable predictive separation. Next-displacement colors overlap in the graph projection, blocked-validation advantage disappeared in the final period, and the graph–ridge uncertainty interval crossed zero. The result supports a key argument in Sheode [1]: a graph is only as useful as the relations encoded in it. Similarity in short histories of one point is not equivalent to mechanical connectivity, and it cannot reconstruct information never measured.

The graph's failure at high-motion intervals is more consequential than the 0.051-mm overall RMSE difference. A method proposed for monitoring can look competitive by

Journal-status statement: It is not under-review at any journal. Subsequent versions may contain substantial revisions arising from community feedback / submission to journal(s). Co-author(s) may be included in future versions. Feedback is welcome. Please feel free to contact the author (via email only). PRE-PRINT VERSION (I): 25.08.2026

THIS MANUSCRIPT IS A NON-PEER-REVIEWED PREPRINT SUBMITTED TO EARTHARXIV.

concentrating predictions near the center of a heavy-tailed series. The event analysis exposed that behavior. Reporting only average error would leave a technically true but operationally misleading impression.

5.2 Relation to spatial graph forecasting

The negative result does not contradict GNSS graph studies [2]– [4]. Those models use multiple monitoring stations and can form edges from spatial relations, correlated movement, or dynamic inter-station structure. Lamosano's released benchmark supplies one selected InSAR point. Its only defensible graph for the present question is temporal-state similarity. The evidence tests a different representation and a much smaller sample.

This distinction suggests a hierarchy for future graph modeling. First, establish the physical or observational entities represented by nodes. Second, justify edge direction and weight independently of forecast success. Third, compare with a non-graph model that receives the same information. Fourth, hold out time periods, sites, or spatial regions that were not used to decide topology. Only then does added graph complexity have an empirical interpretation.

For Lamosano, the next useful extension is not a deeper state network. It is a spatially resolved, openly licensed monitoring stack: multiple InSAR pixels or ground targets, acquisition geometry, uncertainty, rainfall or pore-pressure observations, and terrain-derived flow connectivity. Such a dataset would permit ablation among Euclidean, deformation-correlation, hydrologic, and geology-informed edges. Cross-site validation would then test whether an edge rule transfers rather than merely fits one slope.

5.3 Limitations and engineering implications

Five limitations bound the result. First, the public CSV is short and represents one point, so neither rare-event frequency nor spatial heterogeneity is well sampled. Second, the analysis begins from processed horizontal displacement. It does not propagate interferometric uncertainty or reproduce the upstream SARscape workflow. Third, rainfall is aggregated to

Journal-status statement: It is not under-review at any journal. Subsequent versions may contain substantial revisions arising from community feedback / submission to journal(s). Co-author(s) may be included in future versions. Feedback is welcome. Please feel free to contact the author (via email only). PRE-PRINT VERSION (I): 25.08.2026

the 11-day acquisition interval; intensity, duration, snowmelt, groundwater, and pore pressure are absent. Weak rank correlation cannot be interpreted as rainfall irrelevance. Fourth, the event threshold is a diagnostic quantile, not a geotechnical alarm level. Fifth, the block length and candidate grid were fixed pragmatic choices; broader uncertainty analysis would require more data, not only more resampling.

These limits narrow the engineering conclusion. The state graph can serve as an auditable analogue-retrieval tool or a baseline in a richer study. *It should not be deployed as an early-warning model from this evidence.* For practice, a model should be rejected or escalated for further development when it fails the high-motion gate even if its aggregate RMSE is competitive. Model review should also retain the chronological test boundary and record all topology choices; otherwise, a visually favorable graph can be selected retrospectively.

The published deep-learning RMSE range at Lamosano [5] is lower than the two learned scores reported here, but it is not a common-protocol leaderboard. This study did not rerun those stochastic architectures, and the definitions of R^2 differ. *A fair follow-up would execute all models from controlled open implementations under the same blocked selection, seed policy, and event evaluation. Until then, the defensible statement is limited to the four models actually run.*

6. Conclusion

A causal hydro-kinematic state graph was constructed and tested on the public processed Lamosano InSAR–rainfall record. The graph was selected without access to the final 61 observations and compared with three common baselines. Its test RMSE of 2.451 mm was slightly worse than Ridge-ARX at 2.400 mm, and the 95% moving-block interval for their RMSE difference, −0.084 to 0.200 mm, included zero. Both methods failed to recall all seven training-defined high-motion intervals.

The result is useful precisely because it is negative. A transparent state graph can organize analogue relations in a single-point time series, but that topology did not supply

Journal-status statement: It is not under-review at any journal. Subsequent versions may contain substantial revisions arising from community feedback / submission to journal(s). Co-author(s) may be included in future versions. Feedback is welcome. Please feel free to contact the author (via email only). PRE-PRINT VERSION (I): 25.08.2026

THIS MANUSCRIPT IS A NON-PEER-REVIEWED PREPRINT SUBMITTED TO EARTHARXIV.

dependable new forecast information. It must not be read as a spatial model of the landslide or as an early-warning system. *Future gains should be sought through spatially distributed, uncertainty-aware open monitoring data and physically justified edges, evaluated with site and time holdouts.* The accompanying code, checksum, split definition, and machine-readable outputs make this conclusion directly auditable.

Data and code availability

The processed source data are publicly available from the repository accompanying Nava et al. [5]: https://github.com/lorenzonava96/Landslide-Displacement-Forecasting-using-seven-Deep-Learning-architectures-and-monitoring-data (accessed 21 August 2026). The exact raw-file URL and SHA-256 digest are embedded in the replication script. The source repository did not show a standalone dataset license at the access date; the script downloads rather than redistributes the CSV. The analysis code is released under the MIT License in the accompanying reproducibility package. It contains pinned package versions, all derived result tables, and publication figures. ***Reproducibility package is available from the corresponding author upon reasonable request.***

Author contribution

Mohit Sheode: conceptualization, methodology, software, formal analysis, visualization, data curation, writing—original draft, and writing—review and editing.

Funding

This research received no external funding.

Conflict of interest

The author declares no conflict of interest.

Journal-status statement: It is not under-review at any journal. Subsequent versions may contain substantial revisions arising from community feedback / submission to journal(s). Co-author(s) may be included in future versions. Feedback is welcome. Please feel free to contact the author (via email only). PRE-PRINT VERSION (I): 25.08.2026

References

1. Sheode M., Graph representations for slope instability and landslide kinematics: From fracture networks to physics-informed graph learning. International Journal for Research in Applied Science and Engineering Technology, 14(VII) 2026, pp. 1270–1280. doi:10.22214/ijraset.2026.84294
2. Jiang Y., Luo H., Xu Q., Lu Z., Liao L., Li H. and Hao L., A graph convolutional incorporating GRU network for landslide displacement forecasting based on spatiotemporal analysis of GNSS observations. Remote Sensing, 14(4) 2022, Article 1016, pp. 1–25. doi:10.3390/rs14041016
3. Kuang P., Li R., Huang Y., Wu J., Luo X. and Zhou F., Landslide displacement prediction via attentive graph neural network. Remote Sensing, 14(8) 2022, Article 1919, pp. 1–19. doi:10.3390/rs14081919
4. Li J., Qin J., Kang K., Liang M. and Ding X., Enhanced spatiotemporal landslide displacement prediction using dynamic graph-optimized GNSS monitoring. Sensors, 25(15) 2025, Article 4754, pp. 1–25. doi:10.3390/s25154754
5. Nava L., Carraro E., Reyes-Carmona C., et al., Landslide displacement forecasting using deep learning and monitoring data across selected sites. Landslides, 20 2023, pp. 2111–2129. doi:10.1007/s10346-023-02104-9
6. Teza G., Pesci A., Genevois R. and Galgaro A., Ground-based monitoring of high-risk landslides through joint use of laser scanner and interferometric radar. International Journal of Remote Sensing, 29(16) 2008, pp. 4735–4756. doi:10.1080/01431160801942227
7. Pieraccini M., Casagli N., Luzi G., et al., Integration of radar interferometry and laser scanning for remote monitoring of an urban site built on a sliding slope. IEEE Transactions on Geoscience and Remote Sensing, 44(9) 2006, pp. 2335–2342. doi:10.1109/TGRS.2006.873574
8. Berardino P., Fornaro G., Lanari R. and Sansosti E., A new algorithm for surface deformation monitoring based on small baseline differential SAR interferograms. IEEE Transactions on Geoscience and Remote Sensing, 40(11) 2002, pp. 2375–2383. doi:10.1109/TGRS.2002.803792
9. Cover T. and Hart P., Nearest neighbor pattern classification. IEEE Transactions on Information Theory, 13(1) 1967, pp. 21–27. doi:10.1109/TIT.1967.1053964
10. Künsch H.R., The jackknife and the bootstrap for general stationary observations. The Annals of Statistics, 17(3) 1989, pp. 1217–1241. doi:10.1214/aos/1176347265
11. Harris C.R., Millman K.J., van der Walt S.J., et al., Array programming with NumPy. Nature, 585 2020, pp. 357–362. doi:10.1038/s41586-020-2649-2
12. Virtanen P., Gommers R., Oliphant T.E., et al., SciPy 1.0: Fundamental algorithms for scientific computing in Python. Nature Methods, 17 2020, pp. 261–272. doi:10.1038/s41592-019-0686-2
13. Pedregosa F., Varoquaux G., Gramfort A., et al., Scikit-learn: Machine learning in Python. Journal of Machine Learning Research, 12 2011, pp. 2825–2830.
14. Hunter J.D., Matplotlib: A 2D graphics environment. Computing in Science & Engineering, 9(3) 2007, pp. 90–95. doi:10.1109/MCSE.2007.55